Inorg. Chem. **2003**, *42*, 1193–1203

Structural Modulation of Cu(I) and Cu(II) Complexes of Sterically Hindered Tripyridine Ligands by the Bridgehead Alkyl Groups

Masahito Kodera,* Yuuji Kajita, Yoshimitsu Tachi, and Koji Kano

Department of Molecular Science and Technology, Doshisha University, Kyotanabe, Kyoto 610-0321, Japan

Received September 6, 2002

Structures of Cu(I) and Cu(II) complexes of sterically hindered tripyridine ligands RL = tris(6-methyl-2-pyridyl)-methane (HL), 1,1,1-tris(6-methyl-2-pyridyl)ethane (MeL), and 1,1,1-tris(6-methyl-2-pyridyl)propane (EtL), [Cu(RL)-(MeCN)]PF_6 (**1**–**3**), [Cu(RL)(SO_4)] (**4**–**6**), and [Cu(RL)(NO_3)$_2$] (**7**–**9**), have been explored in the solid state and in solution to gain some insights into modulation of the copper coordination structures by bridgehead alkyl groups (CH, CMe, and CEt). The crystal structures of **1**–**9** show that RL binds a copper ion in a tridentate facial-capping mode, except for **3**, where EtL chelates in a bidentate mode with two pyridyl nitrogen atoms. To avoid the steric repulsion between the bridgehead alkyl group and the 3-H_{py} atoms, the pyridine rings in Cu(I) and Cu(II) complexes of MeL and EtL shift toward the Cu side as compared to those in Cu(I) and Cu(II) complexes of HL, leading to the significant differences in the nonbonding interatomic distances, H···H (between the 3-H_{py} atoms), N···N (between the N_{py} atoms), and C···C (between the 6-Me carbon atoms), the Cu–N_{py}, Cu–N_{MeCN}, and Cu–O bond distances, and the tilt of the pyridine rings. The copper coordination geometries in **4**–**6**, where a SO_4 ligand chelates in a bidentate mode, are varied from a square pyramid of **4** to distorted trigonal bipyramids of **5** and **6**. Such structural differences are not observed for **7**–**9**, where two NO_3 ligands coordinate in a monodentate mode. The structures of **1**–**9** in solution are investigated by means of the electronic, ^{1}H NMR, and ESR spectroscopy. The ^{1}H NMR spectra show that the structures of **1**–**3** in the solid state are kept in solution with rapid coordination exchange of the pyridine rings. The electronic and the ESR spectra reveal the structural changes of **5** and **6** in solution. The bridgehead alkyl groups and 6-Me groups in the sterically hindered tripyridine ligand play important roles in modulating the copper coordination structures.

Introduction

Structural modulations of copper complexes by subtle perturbations of various tridentate and tetradentate ligands have been studied to understand the copper/dioxygen chemistry.[1−7] Karlin et al. first reported a drastic structural effect of length of the tether groups (methyl or ethyl) in TMPA [tris(2-pyridylmethyl)amine] and TEPA [tris(2-pyridylethyl)amine] (Chart 1) on Cu(I)/O_2 reactivity and recently showed more detailed results with a variety of related ligands.[8−15] Suzuki et al. showed that the 6-Me group on pyridine rings in TMPA derivatives drastically affects coordination structures and redox potentials of the copper

* To whom correspondence should be addressed. E-mail: mkodera@mail.doshisha.ac.jp. Phone: +81-774-65-6652. Fax: +81-774-65-6848.

(1) Tyeklár, Z.; Karlin, K. D. *Acc. Chem. Res.* **1989**, *22*, 241.
(2) *Bioinorganic Chemistry of Copper*; Karlin, K. D., Tyeklár, Z., Eds.; Chapman & Hall: New York, 1993.
(3) Kitajima, N.; Moro-oka, Y. *Chem. Rev.* **1994**, *94*, 737.
(4) Tolman, W. B. *Acc. Chem. Res.* **1997**, *30*, 227.
(5) Holland, P. L.; Tolman, W. B. *Coord. Chem. Rev.* **1999**, *190*−*192*, 855.
(6) Blackman, A. G.; Tolman, W. B. *Struct. Bonding (Berlin)* **2000**, *97*, 179.
(7) Schindler, S. *Eur. J. Inorg. Chem.* **2000**, 2311.
(8) Karlin, K. D.; Hayes, J. C.; Juen, S.; Hutchinson, J. P.; Zubieta, J. *Inorg. Chem.* **1982**, *21*, 4106.
(9) Jacobson, R. R.; Tyeklar, Z.; Farooq, A.; Karlin, K. D.; Liu, S.; Zubieta, J. *J. Am. Chem. Soc.* **1988**, *110*, 3690.
(10) Paul, P. P.; Tyeklar, Z.; Jacobson, R. R.; Karlin, K. D. *J. Am. Chem. Soc.* **1991**, *113*, 5322.
(11) Sanyal, I.; Mahroof-Tahir, M.; Nasir, M. S.; Ghosh, P.; Cohen, B. I.; Gultneh, Y.; Cruse, R. W.; Farooq, A.; Karlin, K. D.; Liu, S.; Zubieta, J. *Inorg. Chem.* **1992**, *31*, 4322.
(12) Karlin, K. D.; Wei, N.; Jung, B.; Kaderli, S.; Niklaus, P.; Zuberbühler, A. D. *J. Am. Chem. Soc.* **1993**, *115*, 9506.
(13) Wei, N.; Murthy, N. N.; Chen, Q.; Zubieta, J.; Karlin, K. D. *Inorg. Chem.* **1994**, *33*, 1953.
(14) Karlin, K. D.; Kaderli, S.; Zuberbühler, A. D. *Acc. Chem. Res.* **1997**, *30*, 139.
(15) Schatz, M.; Becker, M.; Thaler, F.; Hampel, F.; Schindler, S.; Jacobson, R. R.; Tyeklár, Z. Murthy, N. N.; Ghosh, P.; Chen, Q.; Zubieta, J.; Karlin, K. D. *Inorg. Chem.* **2001**, *40*, 2312.

10.1021/ic026008m CCC: $25.00 © 2003 American Chemical Society
Published on Web 01/22/2003

Chart 1

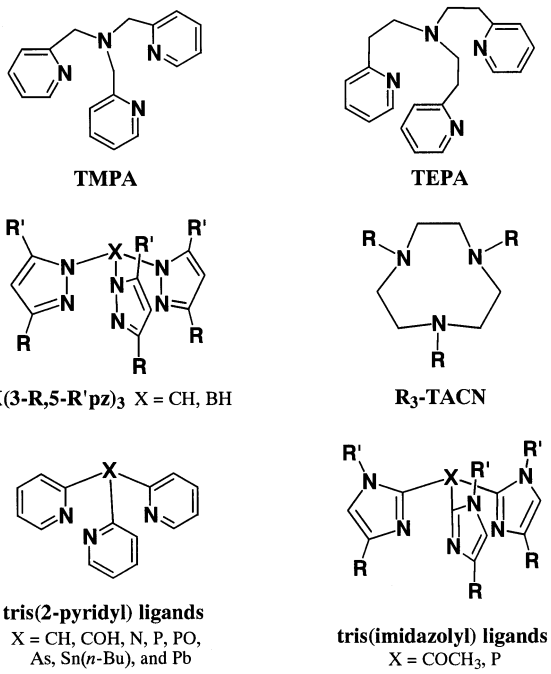

complexes.[16−18] Itoh et al. reported unique effects of a methyl group attached at a tether group in TEPA derivatives.[19,20] 3,5-Bulky alkyl groups of hydrotris(3,5-*R*,*R*′-pyrazolyl)borate ligands (Chart 1) are effective for preventing formation of a bis-ligand mononuclear complex and make the ligands useful to model both monometal and dimetal active sites of metalloproteins, and structural effects of the 3,5-bulky groups on Cu(I) and Cu(II) complexes were reported as well.[21−30] Tolman et al. showed structural effects of bulky alkyl groups and ring sizes in triazamacrocycles (Chart 1) on the stability of μ-η^2:η^2-peroxo- and di-μ-oxodicopper cores.[31,32]

Similar tridentate facial capping ligands based on nitrogen heterocycles, tris(2-pyridyl), tris(pyrazolyl), and tris(imidazolyl) tripod ligands (Chart 1), have contributed to development of the Cu/O_2 chemistry.[33−38] This type of ligand uses various bridgehead groups, CH, COH, N, P, PO, As, B, Sn(*n*-Bu), and Pb, which may be useful for introducing perturbations to the ligands.[39−50] Stack et al. prepared tris(2-pyridyl)methane derivatives systematically modified with methoxy groups at 6-positions on pyridine rings and at the bridgehead position to show drastic effects of the methoxy groups on coordination structures of the Cu(I) and Cu(II) complexes.[51] Durrant et al. used CNHR entities as bridgehead groups of tris(2-pyridyl)methane derivatives to show that the bridgehead N atom acts as a coordination donor.[52] Despite a lot of studies with this type of ligand, the bridgehead alkyl group has never been used for the structural perturbation.

Our interest in this field is the mechanism of reversible O_2-binding by oxyhemocyanin.[53−59] Previously, we reported the crystal structure and reversible O_2-binding of a thermally

(16) Nagao, H.; Komeda, N.; Mukaida, M.; Suzuki, M.; Tanaka, K. *Inorg. Chem.* **1996**, *35*, 6809.
(17) Hayashi, H.; Fujinami, S.; Nagatomo, S.; Ogo, S.; Suzuki, M.; Uehara, A.; Watanabe, Y.; Kitagawa, T. *J. Am. Chem. Soc.* **2000**, *122*, 2124.
(18) Hayashi, H.; Uozumi, K.; Fujinami, S.; Nagatomo, S.; Shiren, K.; Furutachi, H.; Suzuki, M.; Uehara, A.; Kitagawa, T. *Chem. Lett.* **2002**, 416.
(19) Osako, T.; Tachi, Y.; Taki, M.; Fukuzumi, S.; Itoh, S. *Inorg. Chem.* **2001**, *40*, 6604.
(20) Taki, M.; Teramae, S.; Nagatomo, S.; Tachi, Y.; Kitagawa, T.; Itoh, S.; Fukuzumi, S. *J. Am. Chem. Soc.* **2002**, *124*, 6367.
(21) Trofimenko, S. *Chem. Rev.* **1993**, *93*, 943.
(22) Mealli, C.; Arcus, C. S.; Wilkinson, J. L.; Marks, T. J.; Ibers, J. A. *J. Am. Chem. Soc.* **1976**, *98*, 711.
(23) Kitajima, N.; Koda, T.; Hashimoto, S.; Kitagawa, T.; Moro-oka, Y. *J. Am. Chem. Soc.* **1991**, *113*, 5664.
(24) Kitajima, N.; Fujisawa, K.; Fujimoto, C.; Moro-oka, Y.; Hashimoto, S.; Kitagawa, T.; Toriumi, K.; Tatsumi, K.; Nakamura, A. *J. Am. Chem. Soc.* **1992**, *114*, 1277.
(25) Carrier, S. M.; Rugiero, C. E.; Tolman, W. B. *J. Am. Chem. Soc.* **1992**, *114*, 4407.
(26) Carrier, S. M.; Ruggiero, C. E.; Houser, R. P.; Tolman, W. B. *Inorg. Chem.* **1993**, *32*, 4889.
(27) Fujisawa, K.; Tanaka, M.; Moro-oka, Y.; Kitajima, N. *J. Am. Chem. Soc.* **1994**, *116*, 12079.
(28) Fujisawa, K.; Kobayashi, T.; Fujita, K.; Kitajima, N.; Moro-oka, Y.; Miyashita, Y.; Yamada, Y.; Okamoto, K. *Bull. Chem. Soc. Jpn.* **2000**, *73*, 1797.
(29) Hu, Z.; Williams, R. D.; Tran, D.; Spiro, T. G.; Gorun, S. M. *J. Am. Chem. Soc.* **2000**, *122*, 3556.
(30) Hu, Z.; George, G. N.; Gorun, S. M. *Inorg. Chem.* **2001**, *40*, 4812.
(31) Mahapatra, S.; Halfen, J. A.; Wilkinson, E. C.; Pan, G.; Wang, X.; Young, V. G., Jr.; Cramer, C. J.; Que, L., Jr.; Tolman, W. B. *J. Am. Chem. Soc.* **1996**, *118*, 11555.
(32) Lam, B. M. T.; Halfen, J. A.; Young, V. G., Jr.; Hagadorn, J. R.; Holland, P. L.; Lledós, A.; Cucurull-Sánchez, L.; Novoa, J. J.; Alvarez, S.; Tolman, W. B. *Inorg. Chem.* **2000**, *39*, 4059.
(33) Dedert, P. L.; Sorrell, T.; Marks, T. J.; Ibers, J. A. *Inorg. Chem.* **1982**, *21*, 3506.
(34) Sorrell, T.; Borovik, A. S. *J. Am. Chem. Soc.* **1987**, *109*, 4255.
(35) Lynch, W. E.; Kurtz, D. M., Jr.; Wang, S.; Scott, R. A. *J. Am. Chem. Soc.* **1994**, *116*, 11030.
(36) Sorrell, T. N.; Allen, W. E.; White, P. S. *Inorg. Chem.* **1995**, *34*, 952.
(37) Allen, W. E.; Sorrell, T. N. *Inorg. Chem.* **1997**, *36*, 1732.
(38) Kodera, M.; Tachi, Y.; Kita, T.; Kobushi, H.; Sumi, Y.; Kano, K.; Shiro, M.; Koikawa, M.; Tokii, T.; Ohba, M.; Okawa, H. *Inorg. Chem.* **2000**, *39*, 226.
(39) Boggess, R. K.; Zatko, D. A. *Inorg. Chem.* **1976**, *15*, 626.
(40) Szalda, D. J.; Keene, F. R. *Inorg. Chem.* **1986**, *25*, 2795.
(41) Keene, F. R.; Szalda, D. J.; Wilson, T. A. *Inorg. Chem.* **1987**, *26*, 2211.
(42) Hafeli, T. A.; Keene, F. R. *Aust. J. Chem.* **1988**, *41*, 1379.
(43) Keen, F. R.; Snow, M. R.; Stephenson, P. J.; Tiekink, E. R. T. *Inorg. Chem.* **1988**, *27*, 2040.
(44) Keene, F. R.; Stephenson, P. J. *Inorg. Chim. Acta* **1991**, *187*, 217.
(45) Astley, T.; Ellis, P. J.; Freeman, H. C.; Hitchman, M. A.; Keene, F. R.; Tiekink, E. R. T. *J. Chem. Soc., Dalton Trans.* **1995**, 595.
(46) Astley, T.; Headlam, H.; Hitchman, M. A.; Keene, F. R.; Pilbrow, J.; Stratemeier, H.; Tiekink, E. R. T.; Zhong, Y. C. *J. Chem. Soc., Dalton Trans.* **1995**, 3809.
(47) Astley, T.; Hitchman, M. A.; Keene, F. R.; Tiekink, E. R. *J. Chem. Soc., Dalton Trans.* **1996**, 1845.
(48) Adam, K. R.; Anderson, P. A.; Astley, T.; Atkinson, I. M.; Charnock, J. M.; Garner, C. D.; Gulbis, J. M.; Hambley, T. W.; Hitchman, M. A.; Keene, F. R.; Tiekink, E. R. T. *J. Chem. Soc., Dalton Trans.* **1997**, 519.
(49) Szczepura, L. F.; Witham, L. M.; Takeuchi, K. *Coord. Chem. Rev.* **1998**, *174*, 5.
(50) Reger, D. L. *Comments Inorg. Chem.* **1999**, *21*, 1.
(51) Jonas, R. T.; Stack, T. D. P. *Inorg. Chem.* **1998**, *37*, 6615.
(52) Arnold, P. J.; Davies, S. C.; Dilworth, J. R.; Durrant, M. C.; Griffiths, D. V.; Hughes, D. L.; Richards, R. L.; Sharpe, P. C. *J. Chem. Soc., Dalton Trans.* **2001**, 736.
(53) Magnus, K. A.; Hazes, B.; Ton-That, H.; Bonaventura, C.; Bonaventura, J.; Hol, W. G. J. *Proteins: Struct. Funct. Genet.* **1994**, *19*, 302.
(54) Magnus, K. A.; Ton-That, H.; Carpenter, J. E. *Chem. Rev.* **1994**, *94*, 727.
(55) Karlin, K. D.; Cruse, R. W.; Gultneh, Y.; Farooq, A.; Hayes, J. C.; Zubieta, J. *J. Am. Chem. Soc.* **1987**, *109*, 2668.
(56) Karlin, K. D.; Haka, M. S.; Cruse, R. W.; Meyer, G. J.; Farooq, A.; Gultneh, Y.; Hayes, J. C.; Zubieta, J. *J. Am. Chem. Soc.* **1988**, *110*, 1196.
(57) Karlin, K. D.; Tyeklár, Z.; Farooq, A.; Haka, M. S.; Ghosh, P.; Cruse, R. W.; Gultneh, Y.; Hayes, J. C.; Toscano, P. J.; Zubieta, J. *Inorg. Chem.* **1992**, *31*, 1436.
(58) Tyeklár, Z.; Jacobson, R. R.; Wei, N.; Murthy, N. N.; Zubieta, J.; Karlin, K. D. *J. Am. Chem. Soc.* **1993**, *115*, 2677.

Scheme 1

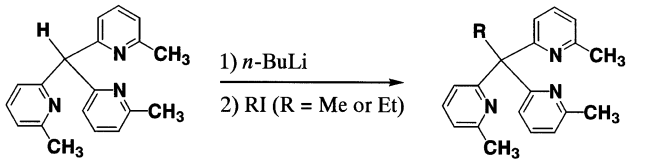

HL R = Me (**MeL**), Et (**EtL**)

stable μ-η^2:η^2-peroxodicopper(II) complex with a sterically hindered hexapyridine ligand, $[Cu_2(O_2)(H6M4h)](PF_6)_2$ (H6M4h = 1,2-bis[2-(bis(6-methyl-2-pyridyl)methyl)-6-pyridyl]ethane), which released an O_2-molecule in MeCN/CH_2Cl_2 upon heating at 80 °C in vacuo, and was regenerated by addition of O_2 at room temperature.[60] On the basis of the crystal structures of a few μ-η^2:η^2-peroxodicopper(II) complexes, we suggested that the Cu coordination structure plays an important role in the reversible O_2-binding.[60] Thus, structural modulation may be important for controlling reversible O_2-binding of the μ-η^2:η^2-peroxodicopper(II) complex. To gain some insights into structural modulations of the copper complexes by subtle perturbations on the tripyridine unit, sterically hindered tripyridine ligands having the various bridgehead groups (CH, CMe, and CEt) {RL = tris(6-methyl-2-pyridyl)methane (HL), 1,1,1-tris(6-methyl-2-pyridyl)ethane (MeL), and 1,1,1-tris(6-methyl-2-pyridyl)-propane (EtL)} have been prepared (Scheme 1), and the structures of Cu(I) and Cu(II) complexes of RL, $[Cu(RL)(MeCN)]PF_6$ {R = H (**1**), Me (**2**), and Et (**3**)}, $[Cu(RL)(SO_4)]$ {R = H (**4**), Me (**5**), and Et (**6**)}, and $[Cu(RL)(NO_3)_2]$ {R = H (**7**), Me (**8**), and Et (**9**)}, have been explored in the solid state and in solution. Here, we report that the coordination structures of the copper complexes can be systematically modulated by the bridgehead alkyl groups, and especially coordination structures of the Cu(II) sulfate complexes **5** and **6** are drastically affected by the bridgehead methyl and ethyl groups, respectively.

Experimental Section

All ordinary reagents and solvents were purchased and used as received unless otherwise noted. Tetrahydrofuran (THF) was dried over sodium metal and distilled. Absolute MeOH was obtained by distillation over Mg. MeCN and CH_2Cl_2 were dried over P_2O_5 and distilled. Tris(6-methyl-2-pyridyl)methane (HL) was prepared by the method reported previously.[38]

Measurements. Elemental analyses (C, H, and N) were carried out at the Elemental Analysis Service Center of Kyoto University. The amounts of copper were analyzed on a Shimazu AA-610 atomic absorption/flame emission spectrophotometer. UV−vis absorption spectra were recorded on a Hitachi U-3210 spectrophotometer. Infrared (IR) spectra were taken on a Shimadzu IR-400 spectrometer with KBr disks. Fast atom bombardment (FAB) mass spectra were obtained on a JEOL JMS-DX 300 spectrometer using *m*-nitrobenzyl alcohol (NBA) as a matrix. ^{1}H NMR spectra in CD_3CN were recorded on a JEOL JMN-A 400 spectrometer by using Me_4Si as an internal standard. ESR spectra were recorded on a JEOL JES-TE 200 spectrometer at 77−298 K. Cyclic voltammograms (CVs) were recorded on a BAS CV-50W voltammetric analyzer. The CV measurements were carried out in CH_2Cl_2 (ca. 1×10^{-3} mol dm^{-3}) using $(Bu_4N)PF_6$ (TBAH) as a supporting electrolyte. A three-electrode cell with a glassy-carbon working electrode, a platinum-coil auxiliary electrode, and a reference electrode Ag/Ag^+ (TBAH/MeCN) was used.

Preparations. 1,1,1-Tris(6-methyl-2-pyridyl)ethane (MeL). In dry THF (200 mL), tris(6-methyl-2-pyridyl)methane (2.89 g, 0.01 mol) was dissolved and degassed by evacuation and refilling with Ar. To the solution was added *n*-butyllithium [(1.6 M in hexane), 6.9 mL, 0.011 mol] at −78 °C. The solution was warmed to room temperature and stirred for 3 h under Ar. The solution was cooled to −78 °C, and CH_3I (1.27 g, 0.010 mol) was added. The mixture was warmed to room temperature and stirred for 15 h under Ar. After the resultant mixture was cooled to room temperature, THF was removed by distillation. To the residue were added 100 mL of $CHCl_3$ and 100 mL of distilled water. The $CHCl_3$ layer was separated, dried over anhydrous Na_2SO_4, and concentrated to dryness. The oily residue was purified by silica gel column chromatography (eluent: $CHCl_3$). MeL (2.90 g, yield 96%) was obtained from the several fractions and recrystallized from *n*-hexane. Mp 122.0−123.6 °C. Anal. Calcd for $C_{20}H_{21}N_3$: C, 79.17; H, 6.98; N, 13.85. Found: C, 78.95; H, 7.06; N, 13.78. UV−vis absorption data (in CH_2Cl_2) [λ_{max}/nm (ϵ_{max}/dm^3 mol^{-1} cm^{-1})]: 267 (10000) and 274 (8400 sh). IR data [ν/cm^{-1}]: 3050 (pyridine C−H), 2950, 2900 (aliphatic C−H), 1585, 1565 (pyridine ring), 1450 (C−H bending), 825, 800, 790, 760, 720, and 690 (pyridine C−H bending). ^{1}H NMR data (δ/ppm vs Me_4Si) in CD_3CN: 7.48 (t, 3H, py-4), 7.03 (d, 3H, py-5), 6.76 (d, 3H, py-3), 2.40 (s, 9H, 6-CH_3-py), and 2.19 (s, 3H, CH_3-C). FAB-MS data: *m*/*z* 304 $[M + H]^+$.

1,1,1-Tris(6-methyl-2-pyridyl)propane (EtL). EtL (yield 82%) was prepared by the same method as MeL using EtI in place of MeI. Mp 86.8−89.8 °C. Anal. Calcd for $C_{21}H_{23}N_3$: C, 79.46; H, 7.30; N, 13.24. Found: C, 78.34; H, 7.36; N, 13.06. UV−vis absorption data (in CH_2Cl_2) [λ_{max}/nm (ϵ_{max}/dm^3 mol^{-1} cm^{-1})]: 268 (9600) and 274 (8300 sh). IR data [ν/cm^{-1}] on KBr disk: 3050 (pyridine C−H), 2950, 2900 (aliphatic C−H), 1580, 1565 (pyridine ring), 1440 (C−H bending), 800, 785, and 775 (pyridine C−H bending). ^{1}H NMR data (δ/ppm vs Me_4Si) in CD_3CN: 7.47 (t, 3H, py-4), 7.04 (d, 3H, py-3), 6.99 (d, 3H, py-5), 2.83 (q, 2H, $-CH_2-$(Et)), 2.39 (s, 9H, 6-CH_3-py), and 0.68 (t, 3H, $-CH_3$ (Et)). FAB-MS data: *m*/*z* 318 $[M + H]^+$.

[Cu(MeCN)(HL)](PF$_6$) (1). MeCN (10 mL) was degassed by a few cycles of evacuation and refilling with Ar, and $[Cu(MeCN)_4](PF_6)$ (41.0 mg, 0.11 mmol) and HL (28.9 mg, 0.1 mmol) were dissolved under Ar. The solution was stirred for 1 h under Ar at room temperature. Upon addition of dry Et_2O to the resultant solution, **1** precipitated as a pale yellow solid. Compound **1** was isolated by filtration (yield 84%) and recrystallized from MeCN/Et_2O to give crystals suitable for X-ray structure analysis. Anal. Calcd for $C_{21}H_{22}N_4PF_6Cu$: C, 46.80; H, 4.11; N, 10.40; Cu, 11.79. Found: C, 46.34; H, 4.12; N, 10.75; Cu, 11.54. UV−vis absorption data (in CH_2Cl_2) [λ_{max}/nm (ϵ_{max}/dm^3 mol^{-1} cm^{-1})]: 273 (8800) and 332 (2200). IR data [ν/cm^{-1}] on KBr disk: 3080 (aromatic C−H), 3000, 2900 (aliphatic C−H), 1595, 1565 (pyridine ring), 1455, 1380 (C−H bending), 840 (PF_6), and 760 (pyridine C−H bending). ^{1}H NMR data (δ/ppm vs Me_4Si) in CD_3CN: 7.76 (t, 3H, py-4), 7.57 (d, 3H, py-3), 7.28 (d, 3H, py-5), 5.94 (s, 1H, methine), and 2.73 (s, 9H, 6-CH_3-py). FAB-MS data: *m*/*z* 393 $[M - PF_6]^+$, 352 $[M - PF_6 - MeCN]^+$.

(59) Lee, D.-H.; Wei, N.; Narasimha, N. M.; Tyeklár, Z.; Karlin, K. D.; Kaderli, S.; Jung, B.; Zuberbühler, A. D. *J. Am. Chem. Soc.* **1995**, *117*, 12498.
(60) Kodera, M.; Katayama, K.; Tachi, Y.; Kano, K.; Hirota, S.; Fujinami, S.; Suzuki, M. *J. Am. Chem. Soc.* **1999**, *121*, 11006.

[Cu(MeCN)(MeL)](PF$_6$) (2). Compound **2** (yield 78%) was synthesized by the same method as **1**, using MeL in place of HL, and recrystallized from MeCN/Et_2O to give crystals suitable for X-ray structure analysis. Anal. Calcd for $C_{22}H_{24}N_4PF_6Cu$: C, 47.78; H, 4.37; N, 10.13; Cu, 11.49. Found: C, 47.70; H, 4.33; N, 10.08; Cu, 11.48. UV−vis absorption data (in CH_2Cl_2) [λ_{max}/nm (ϵ_{max}/dm^3 mol^{-1} cm^{-1})]: 269 (8000) and 342 (2000). IR data [ν/cm^{-1}] on KBr disk: 3100 (aromatic C−H), 2950, 2900 (aliphatic C−H), 1590, 1580 (pyridine ring), 1450, 1380 (C−H bending), 840 (PF_6), and 760 (pyridine C−H bending). ^{1}H NMR data (δ/ppm vs Me_4-Si) in CD_3CN: 7.76 (t, 3H, py-4), 7.66 (d, 3H, py-3), 7.28 (d, 3H, py-5), 2.71 (s, 9H, 6-CH_3-py), and 2.55 (s, 3H, CH_3-C). FAB-MS data: *m*/*z* 391 [M − PF_6 − CH_3]$^+$, 366 [M − PF_6 − MeCN]$^+$.

[Cu(MeCN)(EtL)](PF$_6$) (3). Compound **3** (yield 72%) was synthesized by the same method as **1** using EtL in place of HL and recrystallized from MeCN/Et_2O to give crystals suitable for X-ray structure analysis. Characterization data for **3·H$_2$O** follow. Anal. Calcd for $C_{23}H_{28}N_4PF_6Cu$: C, 47.25; H, 4.83; N, 9.59; Cu, 10.77. Found: C, 47.16; H, 4.39; N, 9.66; Cu, 11.03. UV−vis absorption data (in CH_2Cl_2) [λ_{max}/nm (ϵ_{max}/dm^3 mol^{-1} cm^{-1})]: 277 (8600) and 351 (1400). IR data [ν/cm^{-1}] on KBr disk: 3100 (aromatic C−H), 2950, 2900 (aliphatic C−H), 1590, 1580, 1570 (pyridine ring), 1450, 1380 (C−H bending), 840 (PF_6), and 760 (pyridine C−H bending). ^{1}H NMR data (δ/ppm vs Me_4Si) in CD_3-CN: 7.76 (t, 3H, py-4), 7.37 (d, 3H, py-3), 7.26 (d, 3H, py-5), 2.81(q, 2H, −CH_2− (Et)), 2.51 (s, 9H, 6-CH_3-py), and 0.76 (t, 3H, −CH_3 (Et)). FAB-MS data: *m*/*z* 421 [M − PF_6]$^+$, 380 [M − PF_6 − MeCN]$^+$.

[Cu(SO$_4$)(HL)] (4). $CuSO_4$·$5H_2O$ (25.0 mg, 0.10 mmol) was dissolved in 10 mL of MeOH. To the solution was added a solution of HL (28.9 mg, 0.10 mmol) in MeOH (5 mL), and then, blue solid precipitated immediately. Compound **4** (yield 94%) was isolated as blue powder and recrystallized from MeOH/CH_2Cl_2/Et_2O to give crystals suitable for X-ray structure analysis. Characterization data for **4·MeOH** follow. Anal. Calcd for $C_{19}H_{21}N_3O_4$-SCu: C, 49.99; H, 4.55; N, 8.75; Cu, 13.08. Found: C, 49.82; H, 4.55; N, 8.75; Cu, 13.08. UV−vis reflectance data [λ_{max}/nm]: 710. UV−vis absorption data (in CH_2Cl_2) [λ_{max}/nm (ϵ_{max}/dm^3 mol^{-1} cm^{-1})]: 274 (17000) and 710 (110). IR data [ν/cm^{-1}] on KBr disk: 3050 (aromatic C−H), 2950, 2900 (aliphatic C−H), 1600, 1560 (pyridine ring), 1450, 1380 (C−H bending), 1220, 1140, 1110, 1030, 960, 940 (SO_4), and 820, 770 (pyridine C−H bending). FAB-MS data: *m*/*z* 449 [M]$^+$, 369 [M − SO_3]$^+$, 352 [M − SO_4]$^+$.

[Cu(SO$_4$)(MeL)] (5). Compound **5** (yield 91%) was synthesized by the same method as **4** using MeL in place of HL, and recrystallized from MeOH/CH_2Cl_2 to give crystals suitable for X-ray structure analysis. Anal. Calcd for $C_{20}H_{21}N_3O_4SCu$: C, 51.88; H, 4.57; N, 9.08; Cu, 13.72. Found: C, 51.60; H, 4.48; N, 8.92; Cu, 13.42. UV−vis reflectance data [λ_{max}/nm]: 750. UV−vis absorption data (in CH_2Cl_2) [λ_{max}/nm (ϵ_{max}/dm^3 mol^{-1} cm^{-1})]: 270 (19000) and 614 (80). IR data [ν/cm^{-1}] on KBr disk: 3100 (aromatic C−H), 3000, 2950 (aliphatic C−H), 1600, 1570 (pyridine ring), 1460, 1390 (C−H bending), 1230, 1140, 1030, 950, 930 (SO_4), and 830, 780 (pyridine C−H bending). FAB-MS data: *m*/*z* 463 [M]$^+$, 382 [M − SO_3]$^+$, 366 [M − SO_4]$^+$.

[Cu(SO$_4$)(EtL)] (6). Compound **6** (yield 82%) was synthesized by the same method as **4** using EtL in place of HL and recrystallized from MeOH/CH_2Cl_2/Et_2O to give crystals suitable for X-ray structure analysis. Anal. Calcd for $C_{21}H_{23}N_3O_4SCu$: C, 52.87; H, 4.86; N, 8.81; Cu, 13.32. Found: C, 52.46; H, 4.93; N, 8.58; Cu, 13.34. UV−vis reflectance data [λ_{max}/nm]: 720. UV−vis absorption data (in CH_2Cl_2) [λ_{max}/nm (ϵ_{max}/dm^3 mol^{-1} cm^{-1})]: 268 (17000) and 580 (110). IR data [ν/cm^{-1}] on KBr disk: 3050 (aromatic C−H), 2900 (aliphatic C−H), 1590, 1560 (pyridine ring), 1450, 1370 (C−H bending), 1230, 1140, 1030, 945, 920 (SO_4), and 830, 790, 770 (pyridine C−H bending). FAB-MS data: *m*/*z* 477 [M]$^+$, 380 [M − SO_4]$^+$.

[Cu(NO$_3$)$_2$(HL)] (7). $Cu(NO_3)_2$·$3H_2O$ (24.2 mg, 0.10 mmol) was dissolved in 10 mL of MeOH. To the solution was added a solution of HL (28.9 mg, 0.10 mmol) in MeOH (5 mL). The mixture was stirred for 1 h at room temperature, and pale blue solid precipitated. Compound **7** (yield 88%) was isolated as pale blue powder and recrystallized from MeOH/CH_2Cl_2/Et_2O to give crystals suitable for X-ray structure analysis. Anal. Calcd for $C_{19}H_{19}N_5O_6Cu$: C, 47.85; H, 4.01; N, 14.68; Cu, 13.32. Found: C, 47.02; H, 4.00; N, 14.38; Cu, 12.86. UV−vis reflectance data [λ_{max}/nm]: 710. UV−vis absorption data (in CH_2Cl_2) [λ_{max}/nm (ϵ_{max}/dm^3 mol^{-1} cm^{-1})]: 272 (18000) and 720 (110). IR data [ν/cm^{-1}] on KBr disk: 3050 (aromatic C−H), 2900 (aliphatic C−H), 1600, 1580, 1565 (pyridine ring), 1450 (C−H bending), 1090 (C−O), 840 (PF_6), and 785 (pyridine C−H bending). FAB-MS data: *m*/*z* 414 [M − NO_3]$^+$, 352 [M − $2NO_3$]$^+$.

[Cu(NO$_3$)$_2$(MeL)] (8). Compound **8** (yield 91%) was obtained by the same method as **7** using MeL in place of HL and recrystallized from MeOH/CH_2Cl_2/Et_2O to give crystals suitable for X-ray structure analysis. Anal. Calcd for $C_{20}H_{21}N_5O_6Cu$: C, 48.93; H, 4.31; N, 14.26; Cu, 12.94. Found: C, 48.78; H, 4.32; N, 14.20; Cu, 12.79. UV−vis reflectance data [λ_{max}/nm]: 680. UV−vis absorption data (in CH_2Cl_2) [λ_{max}/nm (ϵ_{max}/dm^3 mol^{-1} cm^{-1})]: 271 (17000) and 690 (110). IR data [ν/cm^{-1}] on KBr disk: 3050 (aromatic C−H), 2900 (aliphatic C−H), 1600, 1580, 1565 (pyridine ring), 1450 (C−H bending), 1090 (C−O), 840 (PF_6), and 785 (pyridine C−H bending). FAB-MS data: *m*/*z* 428 [M − NO_3]$^+$, 366 [M − $2NO_3$]$^+$.

[Cu(NO$_3$)$_2$(EtL)] (9). Compound **9** (yield 90%) was obtained by the same method as **7** using EtL in place of HL and recrystallized from MeOH/CH_2Cl_2/Et_2O to give crystals suitable for X-ray structure analysis. Anal. Calcd for $C_{21}H_{23}N_5O_6Cu$: C, 49.95; H, 4.59; N, 13.87; Cu, 12.58. Found: C, 49.71; H, 4.48; N, 13.82; Cu, 12.61. UV−vis reflectance data [λ_{max}/nm]: 710. UV−vis absorption data (in CH_2Cl_2) [λ_{max}/nm (ϵ_{max}/dm^3 mol^{-1} cm^{-1})]: 270 (19000) and 753 (97). IR data [ν/cm^{-1}] on KBr disk: 3050 (aromatic C−H), 2900 (aliphatic C−H), 1600, 1580, 1565 (pyridine ring), 1450 (C−H bending), 1090 (C−O), 840 (PF_6), and 785 (pyridine C−H bending). FAB-MS data: *m*/*z* 442 [M − NO_3]$^+$, 380 [M − $2NO_3$]$^+$.

Structure Determination of Single Crystals. The structures of **1**−**9** were determined on a Rigaku AFC7R diffractometer with graphite monochromated Mo Kα radiation (λ = 0.71069) and a 12 kW rotating anode generator. Cell constants and an orientation matrix for data collection were typically obtained from a least-squares refinement using the setting angles of 25 carefully centered reflections with 2θ near 25°. Key facets of the structure determinations for the Cu(I) complexes **1**−**3** and the Cu(II) complexes **4**−**9** are given in Tables 1 and 2, respectively. The data were collected at 296(1) K using the ω−2θ scan technique to a maximum 2θ value of 55.0°.

The ω scans of several intense reflections, made prior to data collection, had an average width at half-height of 0.27° with a takeoff angle of 6.0°. Scans of (1.63 + 0.30 tan θ)° were made at a speed of 16.0°/min (in ω). The weak reflections ($I < 10.0\sigma(I)$) were rescanned (maximum of 5 scans), and the counts were accumulated to ensure good counting statistics. Stationary background counts were recorded on each side of the reflection. The ratio of peak counting time to background counting time was 2:1. The computer-controlled slits were set to 3.0 mm (horizontal) and

Table 1. Crystallographic Data for **1**−**3**

	1	**2**	**3**
formula	$C_{21}H_{22}N_4CuPF_6$	$C_{22}H_{24}N_4CuPF_6$	$C_{23}H_{26}N_4CuPF_6$
fw	538.94	552.97	567.00
cryst syst	monoclinic	monoclinic	triclinic
space group	*C2/m* (No. 12)	*C2/m* (No. 12)	$P\bar{1}$ (No. 2)
a/Å	18.889(4)	18.547(3)	10.345(3)
b/Å	14.102(3)	14.025(2)	13.693(2)
c/Å	8.656(3)	8.913(2)	9.439(2)
α/deg			101.88(1)
β/deg	94.92(3)	94.16(2)	96.77(2)
γ/deg			103.21(1)
V/Å^3	2297(1)	2312.2(7)	1254.6(5)
Z	4	4	2
F_{000}	1096	1128	580
T/°C	23	23	23
D_c/g cm^{-3}	1.558	1.588	1.501
cryst size/mm^3	0.40 × 0.20 × 0.15	0.50 × 0.40 × 0.20	0.20 × 0.20 × 0.20
radiation (*λ*/Å)	Mo Kα (0.71069)	Mo Kα (0.71069)	Mo Kα (0.71069)
2*θ* range	20.1° < 2*θ* < 29.2°	29.5° < 2*θ* < 30.0°	21.0° < 2*θ* < 28.2°
scan type	*ω*−2*θ*	*ω*−2*θ*	*ω*−2*θ*
scan width/deg	1.21 + 0.30 tan *θ*	1.63 + 0.30 tan *θ*	0.89 + 0.30 tan *θ*
scan speed/*θ*, deg min^{-1}	16.0	16.0	8.0
no. reflns collcd	2923	2942	6087
no. unique reflns	2746 (R_{int} = 0.065)	2771 (R_{int} = 0.016)	5766 (R_{int} = 0.034)
no. reflns (with)	1066 ($F_o^2 > 2.00\sigma(F_o^2)$)	1988 ($F_o^2 > 3.00\sigma(F_o^2)$)	3308 ($F_o^2 > 3.00\sigma(F_o^2)$)
no. params	196	202	371
refln/param ratio	5.44	9.84	6.62
μ/cm^{-1}	10.85	10.80	9.98
R, R_w [a]	0.046, 0.048	0.038, 0.036	0.043, 0.044
GOF index	1.71	0.90	0.70
final diff ρ_{max}/e Å^{-3}	+0.36; −0.29	+0.56; −0.43	+1.50; −1.17

[a] $R = \sum||F_o| - |F_c||/\sum|F_o|$. $R_w = [\sum w(|F_o| - |F_c|)^2/\sum w(F_o)^2]^{1/2}$, where $w = 1/\sigma^2(F_o)$.

Table 2. Crystallographic Data for **4**−**9**

	4	**5**	**6**	**7**	**8**	**9**
formula	$C_{19}H_{19}N_3O_5SCu$	$C_{20}H_{21}N_3O_4SCu$	$C_{21}H_{23}N_3O_4SCu$	$C_{19}H_{19}N_5O_6Cu$	$C_{20}H_{21}N_5O_6Cu$	$C_{21}H_{23}N_5O_6Cu$
fw	464.98	463.01	477.04	476.93	490.69	504.99
cryst syst	orthorhombic	triclinic	monoclinic	monoclinic	monoclinic	monoclinic
space group	*Pbcm* (No. 57)	$P\bar{1}$ (No. 2)	$P2_1/n$ (No. 14)	$P2_1$/c (No. 14)	$P2_1$ (No. 4)	$P2_1/n$ (No. 14)
a/Å	8.422(3)	9.142(3)	9.265(1)	8.570(2)	8.222(3)	9.441(2)
b/Å	18.193(3)	13.708(4)	16.130(3)	13.921(2)	13.983(4)	13.859(2)
c/Å	13.876(3)	8.239(3)	14.170(2)	16.878(1)	9.332(3)	16.699(4)
α/deg		90.54(2)				
β/deg		104.40(3)	101.83(1)	97.30(1)	103.24(3)	90.64(2)
γ/deg		103.02(2)				
V/Å^3	2126.0(8)	972.0(6)	2072.6(5)	1997.3(5)	1044.4(6)	2184.8(7)
Z	4	2	4	4	2	4
F_{000}	956	478	988	980	506	1044
T/°C	20	20	23	23	20	23
D_c/g cm^{-3}	1.453	1.582	1.529	1.586	1.561	1.535
cryst size/mm^3	0.10 × 0.40 × 0.40	0.40 × 0.40 × 0.20	0.20 × 0.20 × 0.30	0.30 × 0.35 × 0.20	0.60 × 0.50 × 0.40	0.20 × 0.50 × 0.70
radiation (*λ*/Å)	Mo Kα (0.71069)	Mo Kα (0.71069)	Mo Kα (0.71069)	Mo Kα (0.71069)	Mo Kα (0.71069)	Mo Kα (0.71069)
2*θ* range	27.8° < 2*θ* < 29.9°	28.7 < 2*θ* < 30.0	27.2 < 2*θ* < 29.8	29.3 < 2*θ* < 30.0	28.8 < 2*θ* < 29.7	27.2 < 2*θ* < 29.8
scan type	*ω*−2*θ*	*ω*−2*θ*	*ω*−2*θ*	*ω*−2*θ*	*ω*−2*θ*	*ω*−2*θ*
scan width/deg	1.73 + 0.30 tan *θ*	1.15 + 0.30 tan *θ*	0.94 + 0.30 tan *θ*	1.31 + 0.30 tan *θ*	1.31 + 0.30 tan *θ*	1.42 + 0.30 tan *θ*
scan speed/*θ*, deg min^{-1}	16.0	16.0	16.0	16.0	16.0	16.0
no. reflns collcd	2786	4738	4087	5086	2668	5533
no. unique reflns		4456 (R_{int} = 0.010)	3819 (R_{int} = 0.034)	4777 (R_{int} = 0.037)	2504 (R_{int} = 0.014)	5228 (R_{int} = 0.032)
no. reflns (with)	1078 ($F_o^2 > 3.00\sigma(F_o^2)$)	3854 ($F_o^2 > 3.00\sigma(F_o^2)$)	1800 ($F_o^2 > 3.00\sigma(F_o^2)$)	2491 ($F_o^2 > 3.00\sigma(F_o^2)$)	2369 ($F_o^2 > 2.00\sigma(F_o^2)$)	2782 ($F_o^2 > 3.00\sigma(F_o^2)$)
no. params	150	263	272	281	289	299
refln/param ratio	7.19	14.65	6.62	8.86	8.20	9.30
μ/cm^{-1}	11.60	12.64	11.88	11.42	10.95	10.49
R, R_w [a]	0.068, 0.080	0.034, 0.035	0.046, 0.050	0.037, 0.038	0.040, 0.041	0.039, 0.040
GOF index	1.48	1.14	2.16	0.74	1.99	0.54
final diff ρ_{max}/e Å^{-3}	+1.12; −0.52	+0.38; −0.40	+5.99; −2.66	+0.74; −0.37	+1.03; −0.57	+0.60; −0.66

[a] $R = \sum||F_o| - |F_c||/\sum|F_o|$. $R_w = [\sum w(|F_o| - |F_c|)^2/\sum w(F_o)^2]^{1/2}$, where $w = 1/\sigma^2(F_o)$.

3.0 mm (vertical). The intensities of three representative reflections were measured after every 150 reflections. No decay correction was applied. All nine structures were solved by direct methods (SHELEXS 86, SIR 92, SAPI 91, and SHELEXS 97) and expanded

using Fourier techniques. All non-hydrogen atoms were refined anisotropically. Hydrogen atoms were included but not refined. The function minimized was $\sum w(|F_o| - |F_c|)^2$ with $w = 1$. The neutral atom scattering factors were taken from Cromer and Waver.[61] Anomalous dispersion effects were included in F_c,[62] the values for $\Delta f'$ and $\Delta f''$ being taken from the reference[63] and those for the mass-attenuation coefficients.[64] All calculations were performed using the teXan crystallographic software package.[65] The following information is available in the Supporting Information: a packing diagram of the unit cell and a complete set of crystallographic tables including positional parameters, anisotropic thermal factors, bond lengths, and bond angles.

Results and Discussion

Preparation of RL. The sterically hindered tripyridine ligands, RL (R = H, Me, and Et), are synthesized. HL is prepared according to the previous method.[38] MeL and EtL, which have bridgehead methyl and ethyl groups, are derived from HL via lithiation with *n*-BuLi at the bridgehead methine position and subsequent alkylation with MeI and EtI, respectively.

Syntheses of the Cu(I) and Cu(II) Complexes 1−9. The Cu(I) complexes [Cu(MeCN)(RL)](PF_6) {R = H (**1**), Me (**2**), and Et (**3**)} are anaerobically synthesized from RL and [Cu(MeCN)$_4$](PF_6) in MeCN. Once isolated, the Cu(I)−MeCN complexes of RL are stable under air in the solid state and in MeCN and can be recrystallized from MeCN/Et_2O under air. The coordination of MeCN protects **1**−**3** from O_2-oxidation.[19,51] The Cu(I) complexes **1**−**3**, however, are slowly oxidized to green Cu(II) species under air at room temperature in CH_2Cl_2 without apparent generation of μ-η^2:η^2-peroxodicopper(II) complexes. The reactions of **1**−**3** with O_2 are followed by the electronic absorption spectra at room temperature for three weeks, but any intermediate is not observed at all. The spectra of the final resultant mixtures show broad bands at 600−700 nm due to d−d transitions of Cu(II). The MeCN ligand of **1**−**3** can be substituted by triphenylphosphine (PPh_3) and carbon monooxide (CO) in CH_2Cl_2. The resultant Cu(I)−PPh_3 and Cu(I)−CO complexes of RL are resistant to O_2-oxidation in various solvents. The Cu(I) complexes **1**−**3** are characterized by the UV−vis and ^{1}H NMR spectroscopy and X-ray analysis. The Cu(II) complexes [Cu(RL)(SO_4)] {R = H (**4**), Me (**5**), and Et (**6**)}, and [Cu(RL)(NO_3)$_2$] {R = H (**7**), Me (**8**), and Et (**9**)} are quantitatively obtained from reactions of RL with $CuSO_4$·$5H_2O$ and Cu(NO_3)$_2$·$3H_2O$ in MeOH and are characterized by X-ray analysis, UV−vis, ESR spectroscopy, and cyclic voltammetry.

In the previous paper, we reported that HL is oxygenated at the bridgehead methine position to afford MeOL (methoxy derivatives), HOL (hydroxy derivatives), and bpk (bis(6-methyl-2-pyridyl)ketone) upon aerobic reactions of HL with CuX_2 (X = Cl and Br) in MeOH and also autoxidized to HOL and bpk upon aerobic reactions with catalytic amounts of various Cu(II) salts, such as $CuSO_4$·$5H_2O$ and Cu(NO_3)$_2$·$3H_2O$.[38] In the former reaction, halogenation of HL occurs at the bridgehead methine position, and the resultant XL (X = Cl and Br) is converted to MeOL via substitution reaction with MeOH. The autoxidation of HL catalyzed by the Cu(II) ion may proceed via a bridgehead carbon radical intermediate ·L. On the other hand, stoichiometric reactions of HL with $CuSO_4$·$5H_2O$ and Cu(NO_3)$_2$·$3H_2O$, a 1:1 ratio of HL/Cu salt, afford the Cu(II) complexes **4** and **7** quantitatively, respectively. The generation of ·L may be inhibited in the stoichiometric complexation because the complexation fixes a tetrahedral configuration of the bridgehead methine carbon in HL to destabilize a planar configuration required for ·L. The metal free HL, being more reactive in the autoxidation, does not remain in the stoichiometric reaction. These may be reasons for the quantitative formation of **4** and **7** in the stoichiometric reaction. MeL and EtL, having the bridgehead methyl and ethyl groups, respectively, are not oxidized upon aerobic reactions with the Cu(I) and Cu(II) salts, to give the corresponding Cu(I) and Cu(II) complexes quantitatively.

RL ligands stabilize the mono-ligated Cu(I) and Cu(II) complexes in the solid state and in solution but do not form bis-ligated complexes at all even under conditions of excess ligand due to the steric hindrance of the Me groups at the 6-positions of pyridine rings. Stack et al. reported a similar feature with a sterically hindered tripyridine ligand MeOL-(OMe)$_3$ (tris(6-methoxy-2-pyridyl)methoxymethane) in a facial-capping *N*,*N*′,*N*″ coordination mode, where MeOL-(OMe)$_3$ has four MeO groups; three of them are at 6-positions of three pyridine rings, and another is at the bridgehead site. However, MeOL(OMe)$_3$ forms a bis-ligated complex in a facial-capping *N*,*N*′,*O* coordination mode because the oxygen atom of the bridgehead methoxy group in MeOL(OMe)$_3$ can participate in the coordination.[51] Therefore, the 6-Me and the bridgehead alkyl groups of RL are more effective in preventing the formation of the bis-ligated complex than the MeO groups of MeOL(OMe)$_3$.

Crystal Structures of 1−9. Crystal structures of three Cu(I) complexes **1**−**3** and six Cu(II) complexes **4**−**9** have been determined. The Cu(I) complexes are composed of a complex cation [Cu(RL)(MeCN)]$^+$ and a counteranion PF_6, while for the Cu(II) complexes, the Cu(II) ion is coordinated by counteranions (X = SO_4 and $2NO_3$) to form neutral complexes [Cu(RL)(X)]. The crystal structures reveal that RL coordinates with three pyridine rings in a facial capping mode, except for **3**, where EtL chelates in a bidentate mode with two pyridyl nitrogen atoms. Significant steric effects of the bridgehead alkyl groups on the copper coordination structures are observed in the crystal structures. Crystal parameters and important data collection for the Cu(I) and Cu(II) complexes are summarized in Tables 1 and 2, respectively.

ORTEP diagrams of the cations [Cu(MeCN)(RL)]$^+$ (R = H, Me, and Et) of **1**−**3** are shown in Figure 1. The selected

(61) Cromer, D. T.; Waber, J. T. *International Tables for X-ray Crystallography*; Kynoch Press: Birmingham, U.K., 1974; Vol. 4.
(62) Ibers, J. A.; Hamilton, W. C. *Acta Crystallogr.* **1964**, *17*, 781.
(63) Creagh, D. C.; McAuley, W. J. *International Tables for X-ray Crystallography*; Kluwer: Boston, 1992.
(64) Creagh, D. C.; Hubbell, H. H. *International Tables for X-ray Crystallography*; Kluwer: Boston, 1992.
(65) *Single crystal structure analysis software*, version 1.6: Molecular Structure Corp.; The Woodlands, TX, 1993.

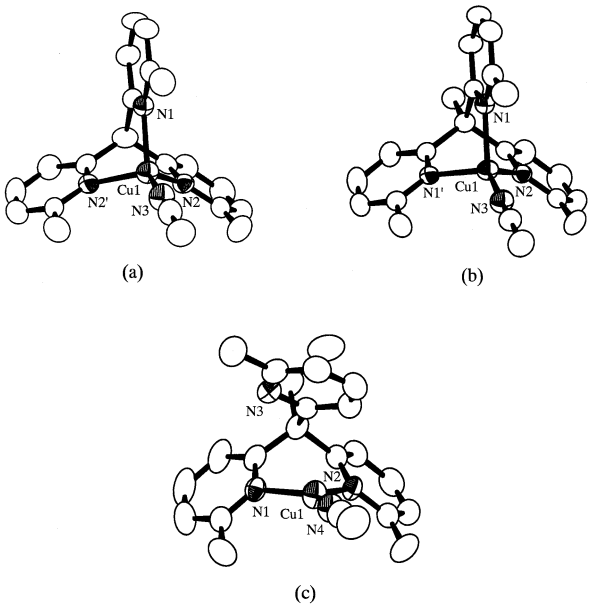

Figure 1. ORTEP views of the cationic portions of the Cu(I) complexes **1** (a), **2** (b), and **3** (c) with the atom numbering scheme (50% probability ellipsoids).

Table 3. Selected Bond Distances (Å) and Angles (deg) for **1**−**3**

1		**2**		**3**	
Cu1−N1	2.088(7)	Cu1−N1	2.067(2)	Cu1−N1	2.021(4)
Cu1−N2	2.083(5)	Cu1−N2	2.053(3)	Cu1−N2	2.039(4)
Cu1−N3	1.883(8)	Cu1−N3	1.900(4)	Cu1−N4	1.881(4)
N1−Cu1−N2	91.1(2)	N1−Cu1−N1′	91.6(1)	N1−Cu1−N2	91.7(2)
N1−Cu1−N3	126.8(3)	N1−Cu1−N2	90.23(9)	N1−Cu1−N4	135.4(2)
N2−Cu1−N2′	91.8(3)	N1−Cu1−N3	124.15(9)	N2−Cu1−N4	132.4(2)
N2−Cu1−N3	123.1(2)	N2−Cu1−N3	126.0(2)		

bond distances and bond angles of **1**−**3** are shown in Table 3. Each cation of **1** and **2** lies on a crystallographic symmetry plane containing the Cu(I) ion, a single pyridine ring, the bridgehead group (CH and CMe), and the MeCN ligand, and each asymmetric unit contains a half of the cation, while the cation of **3** has no symmetry, and the asymmetric unit contains the whole cation. The Cu(I) ion in **1** assumes a nearly C_3 symmetric trigonal pyramidal geometry with three pyridyl nitrogen atoms of HL coordinating in a facial-capping mode and with a fourth MeCN ligand; the Cu−N_{py} bond distances and the N_{py}−Cu−N_{py} bond angles for **1** are almost equivalent (Table 3). The dihedral angles between the pyridine rings in **1** are exactly 120°. In the crystal structures, **2** is similar to **1** as shown in Figure 1a,b though the bridgehead methyl in **2** causes significant structural differences between **1** and **2**.

The pyridine rings in **2** shift toward the Cu side as compared to those in **1**, due to the steric repulsion between the bridgehead methyl group and the 3-H_{py} atoms. The pyridine shift in **2** is schematically drawn in Figure 2 in comparison with **1**. The pyridine shift between **1** and **2** is estimated from differences of the average nonbonding interatomic distances, H···H (the 3-H_{py} atoms), N···N (the N_{py} atoms), and C···C (the 6-Me carbon atoms). The H···H, N···N, and C···C of **1**−**9** are shown in Supporting Information. The H···H in **2** is longer by 0.199 Å, and the N···N and the C···C in **2** are shorter by 0.048 and 0.193 Å,

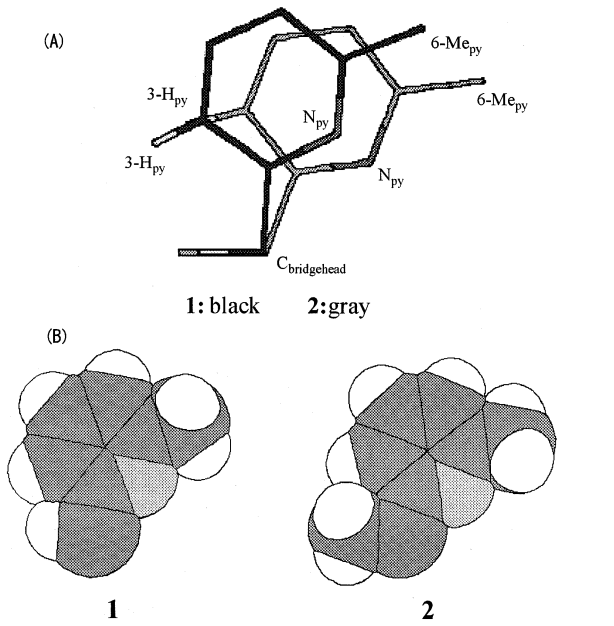

Figure 2. Pyridine shift of **2** compared with **1** (A) and the steric repulsion between the 5-H_{py} atoms and the bridgehead groups represented by the space-filling models of the pyridine parts of **1** and **2** (B) are drawn on the basis of the crystal structures of **1** and **2**.

respectively, than the comparable distances in **1**. The pyridine shift leads to subtle differences in the bond distances around Cu(I) ions; the average Cu−N_{py} bond distance in **2** is shorter by 0.022 Å than the comparable distance in **1**, and the Cu−N_{MeCN} bond distance in **2** is longer by 0.017 Å than the comparable distance in **1**. The differences of the Cu−N_{py} bond distances in **1** and **2** suggest that the strength of ligand field given by RL increases with increasing size of the bridgehead groups. Considering the elongation of the Cu−N_{MeCN} bond distances, the steric hindrance by the 6-Me groups may be enhanced by the pyridine shift. The Cu−N_{MeCN} bond distance in **2** is longer by 0.015 Å than the comparable distance in the Cu(I) complex of $MeOL(OMe)_3$, $[Cu(MeCN)(MeOL(OMe)_3)](OTf)$ (**10**), reported by Stack et al.[51] The 6-Me in **2** provides greater steric hindrance than the MeO groups in **10**. This is because the Me group in **2** is larger than the oxygen atom of MeO in **10**. What is critical in the steric hindrance of the MeO group is not the overall size of the MeO group, but the size of the oxygen atom directly attached. The copper coordination geometry in **3** is drastically different from those in **1** and **2** due to the bridgehead ethyl group (see Figure 1). The Cu(I) ion in **3** assumes a triangular geometry with two pyridyl nitrogen atoms of EtL chelating in a bidentate mode and with a third MeCN ligand. The triangular geometry in **3** is more distorted than the pseudotetrahedral geometry in **10**, suggesting that the 6-Me groups exert a more drastic effect upon the copper coordination geometry than the 6-MeO groups. The Cu−N_{py} bond distances of **3** are shorter by 0.056 Å on average than those of **1**. This is due to the small coordination number of **3** (three coordinate) as compared to **1** (four coordinate). In conclusion, the bridgehead alkyl groups affect the coordination structures of the Cu(I) complexes through the steric repulsion to the 3-H_{py} atoms, and also enhance the steric hindrance of the 6-Me groups.

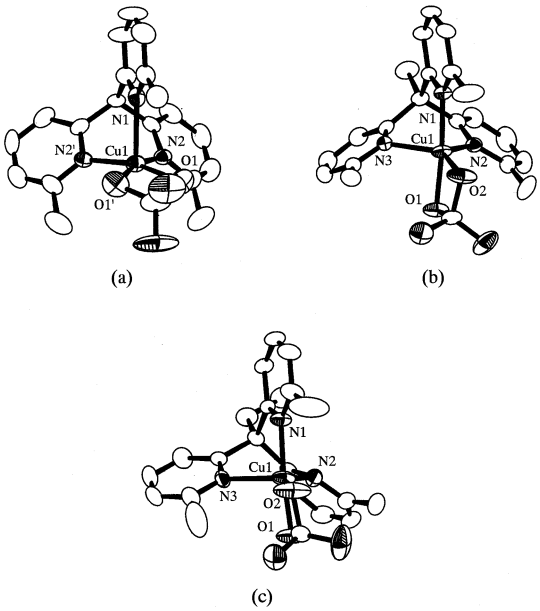

Figure 3. ORTEP views of the Cu(II) sulfate complexes **4** (a), **5** (b), and **6** (c) with the atom numbering scheme (50% probability ellipsoids).

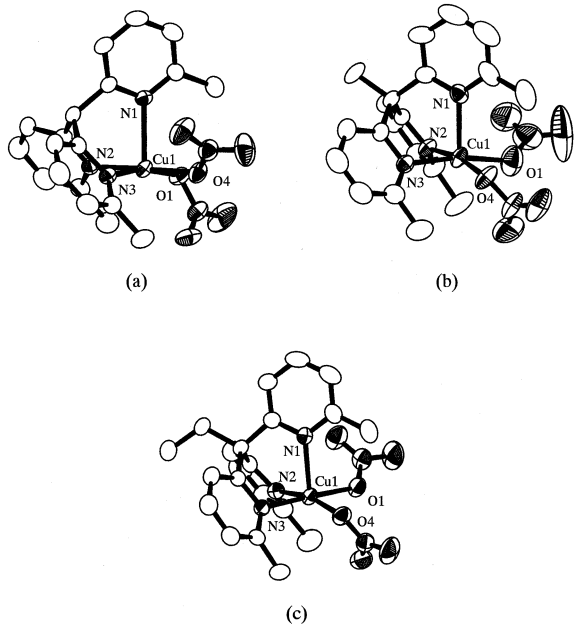

Figure 4. ORTEP views of the Cu(II) nitrate complexes **7** (a), **8** (b), and **9** (c) with the atom numbering scheme (50% probability ellipsoids).

ORTEP diagrams of $[Cu(SO_4)(RL)]$ (R = H (**4**), Me (**5**), and Et (**6**)) and of $[Cu(NO_3)_2(RL)]$ (R = H (**7**), Me (**8**), and Et (**9**)) are shown in Figures 3 and 4, and the selected bond distances and bond angles of **4**−**6** and **7**−**9** are shown in Tables 4 and 5, respectively. The Cu(II) sulfate complex of HL (**4**) lies on a crystallographic symmetry plane containing the Cu(II) ion, a single pyridine ring, the bridgehead CH, and the sulfur and two oxygen atoms of the sulfate ligand, and the asymmetric unit contains a half of the complex. Other Cu(II) sulfate (**5** and **6**) and nitrate (**7**−**9**) complexes have no symmetry, and the asymmetric units contain the entire complexes. The Cu(II) ions in **4**−**9** assume five coordinate structures with three nitrogen atoms of the pyridine rings and with two oxygen atoms of the sulfate ligand for **4**−**6** or of two nitrate ligands for **7**−**9**, where the sulfate ligand chelates in a bidentate mode while the nitrate ligands coordinate in a monodentate mode.

Table 4. Selected Bond Distances (Å) and Angles (deg) for **4**−**6**

4		**5**		**6**	
Cu1−O1	1.976(8)	Cu1−O1	1.980(2)	Cu1−O1	1.980(5)
Cu1−N1	2.28(1)	Cu1−O2	2.028(2)	Cu1−O2	1.974(5)
Cu1−N2	2.022(8)	Cu1−N1	2.001(2)	Cu1−N1	1.993(5)
		Cu1−N2	2.112(2)	Cu1−N2	2.073(5)
		Cu1−N3	2.119(2)	Cu1−N3	2.225(6)
O1−Cu1−O1′	72.0(5)	O1−Cu1−O2	69.81(8)	O1−Cu1−O2	91.7(2)
O1−Cu1−N1	101.4(4)	O1−Cu1−N1	175.0(1)	O1−Cu1−N1	174.7(3)
O1−Cu1−N2	98.8(3)	O1−Cu1−N2	97.91(9)	O1−Cu1−N2	92.9(2)
O1−Cu1−N2′	164.9(3)	O1−Cu1−N3	91.36(9)	O1−Cu1−N3	99.2(2)
N1−Cu1−N2	92.0(3)	O2−Cu1−N1	132.3(1)	O2−Cu1−N1	109.9(2)
N2−Cu1−N2′	87.5(5)	O2−Cu1−N2	126.4(1)	O2−Cu1−N2	140.3(3)
		N1−Cu1−N2	85.81(9)	N1−Cu1−N2	84.5(3)
		N1−Cu1−N3	84.75(8)	N1−Cu1−N3	85.7(2)
		N2−Cu1−N3	98.58(9)	N2−Cu1−N3	97.2(2)

Table 5. Selected Bond Distances (Å) and Angles (deg) for **7**−**9**

7		**8**		**9**	
Cu1−O1	1.992(3)	Cu1−O1	1.969(5)	Cu1−O1	2.005(3)
Cu1−O4	1.995(3)	Cu1−O4	1.969(3)	Cu1−O4	1.979(3)
Cu1−N1	2.291(3)	Cu1−N1	2.247(5)	Cu1−N1	2.267(3)
Cu1−N2	2.058(3)	Cu1−N2	1.982(4)	Cu1−N2	1.976(3)
Cu1−N3	2.003(3)	Cu1−N3	2.048(5)	Cu1−N3	2.029(3)
O1−Cu1−O4	83.8(1)	O1−Cu1−O4	83.8(2)	O1−Cu1−O4	86.9(1)
O1−Cu1−N1	97.0(1)	O1−Cu1−N1	99.8(2)	O1−Cu1−N1	93.5(1)
O1−Cu1−N2	93.3(1)	O1−Cu1−N2	99.2(2)	O1−Cu1−N2	95.6(1)
O1−Cu1−N3	166.8(1)	O1−Cu1−N3	170.3(2)	O1−Cu1−N3	178.1(1)
O4−Cu1−N1	93.5(1)	O4−Cu1−N1	95.6(2)	O4−Cu1−N1	98.8(1)
O4−Cu1−N2	177.0(1)	O4−Cu1−N2	168.8(3)	O4−Cu1−N2	165.4(1)
O4−Cu1−N3	96.5(1)	O4−Cu1−N3	91.3(2)	O4−Cu1−N3	93.2(1)
N1−Cu1−N2	87.8(1)	N1−Cu1−N2	94.6(2)	N1−Cu1−N2	95.4(1)
N1−Cu1−N3	96.2(1)	N1−Cu1−N3	89.0(2)	N1−Cu1−N3	88.5(1)
N2−Cu1−N3	86.0(1)	N2−Cu1−N3	84.0(2)	N2−Cu1−N3	83.9(1)

Table 6. Differences in the Average Values of Nonbonding Interatomic Distances between the Copper Complexes of RL (R = Me or Et) and of HL

	differences (Å)		
cmpd	H···H	C···C	N···N
$\mathbf{2}_{MeL} - \mathbf{1}_{HL}$	0.199	−0.193	−0.048
$\mathbf{5}_{MeL} - \mathbf{4}_{HL}$	0.332	−0.241	−0.068
$\mathbf{6}_{EtL} - \mathbf{4}_{HL}$	0.317	−0.184	−0.053
$\mathbf{8}_{MeL} - \mathbf{7}_{HL}$	0.260	−0.155	−0.058
$\mathbf{9}_{EtL} - \mathbf{7}_{HL}$	0.220	−0.183	−0.059

The pyridine rings shift toward the Cu(II) side due to the steric repulsion between the bridgehead alkyl groups and the 3-H_{py} atoms in the Cu(II) complexes as found in the Cu(I) complexes. The difference data for the nonbonding interatomic distances H···H, N···N, and C···C in the Cu(I) and Cu(II) complexes are shown in Table 6. The difference data in the Cu(II) complexes are close to the corresponding values in the Cu(I) complexes of MeL and HL, indicating that the pyridine shifts in the Cu(II) complexes are similar to that in the Cu(I) complexes of MeL and HL. The absolute difference values of H···H, N···N, and C···C in the Cu(II) complexes of EtL and HL are slightly smaller than those in the Cu(II) complexes of MeL and HL, except for the C···C in the Cu(II) nitrate complexes. For the pyridine shifts, the bridgehead methyl group is slightly more effective than the bridgehead ethyl group.

The pyridine shifts lead to significant differences in the bond distances around the Cu(II) ion. With the bridgehead

alkyl groups, the Cu−N_{py} bond distances in the Cu(II) complexes are shortened similarly to those of the Cu(I) complexes. The average Cu−N_{py} bond distances in **5** and **6** are shorter by 0.031 and 0.011 Å than that in **4**, and those in **8** and **9** are shorter by 0.025 and 0.026 Å than that in **7**, respectively (Tables 4 and 5). On the other hand, the changes of the Cu−O bond distances induced by the bridgehead alkyl groups are complicated. The average Cu−O bond distances in **5** and **6** are longer by 0.028 and 0.001 Å than that in **4** while those in **8** and **9** are shorter by 0.025 and 0.002 Å than that in **7**, respectively. The average Cu−O bond distances are elongated by the bridgehead alkyl groups in the sulfate complexes, but shortened in the nitrate complexes. The difference between the sulfate and the nitrate complexes may be caused by the copper coordination geometry. The coordination geometry is estimated from the τ values. The τ values vary from 0, for an idealized square pyramid, to 1, for an idealized trigonal bipyramid.[66] Judging from the τ values, 0, 0.71, and 0.58 for **4**, **5**, and **6**, respectively, the coordination geometry in the sulfate complexes is varied from the idealized square pyramid to the distorted trigonal bipyramid. On the other hand, the coordination geometry in the nitrate complexes is not affected by the bridgehead alkyl groups and is all distorted square pyramid similar to one another because the τ values of **7**, **8**, and **9** are 0.17, 0.025, and 0.21, respectively. The change of the coordination geometry in the sulfate complexes is clearly shown by the ORTEP drawings in Figure 3; the O(1)−Cu−O(1′) plane is nearly parallel to the N(2)−Cu−N(2′) plane in **4** (Figure 3a), but the O(1)−Cu−O(2) plane is perpendicular to the N(2)−Cu−N(3) plane in **5** and **6** (Figure 3b,c). To avoid the steric hindrance of the 6-Me groups enhanced by the bridgehead alkyl groups, the chelate rings of Cu(II) sulfate in **5** and **6** have to vary the configuration around the Cu(II) ion, leading to the drastic change of the coordination geometry. On the other hand, the monodentate nitrate ligands in **8** and **9** can avoid the steric hindrance of the 6-Me groups only by the conformational change along the N−O bond in the nitrate ligands, resulting in the subtle change of coordination geometry (see Figure 4). Thus, the bridgehead alkyl groups specifically affect the chelate ring of the Cu(II) sulfate through the steric repulsion between the 6-Me groups and the Cu(II) sulfate chelate ring, resulting in the dramatic change of the copper coordination geometry and elongation of the Cu−O bond distances.

The pyridine rings in **3**, **5**, **6**, **8**, and **9**, which have the bridgehead alkyl groups, are tilted by the steric effect of the bridgehead alkyl groups. The tilt of the pyridine rings can be estimated from the $R_{(H\ or\ C)}$−$C_{bridgehead}$−C_{2-py}−N_{py} dihedral angles, the ideal value of which is 180°. Durrant et al. estimated the tilt of the pyridine rings in various metal complexes of tripyridine type ligands from the Cu−N_{py}−C_{4-py} angles, which are angles between the Cu−N_{py} bond and the N_{py}−C_{4-py} diagonal of the pyridine ring, with ideal value 180°.[52] These two angles of **1**−**9** are shown in Table 7. The dihedral angle and the Cu−N_{py}−C_{4-py} angle for the pyridine ring free from coordination in **3** are 72.8° and 71.5°, respectively, and the angles for all pyridine rings in **1** and **2** are in the range 170−180°. This indicates that the tilt of the pyridine ring is reasonably estimated from the two angles. The two angles in **1**−**9** are gradually decreased from idealized 180° with increasing the size of bridgehead groups (CH, CMe, and CEt) as shown in Table 7, indicating that the bridgehead alkyl groups directly affect the orientation of the pyridine rings.[52] Stack et al. showed that the dihedral angles between the pyridine rings in Cu(I) and Cu(II) complexes of tripyridine type ligands having bridgehead methoxy group depend on the positioning of methyl group in the bridgehead methoxy group.[51] A similar steric effect is observed for the copper complexes of EtL; one of three dihedral angles between the pyridine rings, 128.1° for **6**, the Cu(II) sulfate complex of EtL, and 131.72° for **9**, the Cu(II) nitrate complex of EtL, are larger than the other two angles, 110.86° and 113.38° for the former and 112.42° and 112.53° for latter. Thus, the bridgehead ethyl group behaves similarly to the bridgehead methoxy group to induce a larger tilt of the pyridine rings.

Table 7. Two Angles (deg) ($R_{(H\ or\ C)}$−$C_{bridgehead}$−C_{2-py}−N_{py} and Cu−N_{py}−C_{4-py}) of **1**−**9**

cmpd	$R_{(H\ or\ C)}$−$C_{bridgehead}$−C_{2-py}−N_{py}	Cu−N_{py}−C_{4-py}
1	180.0, 170.3, 170.3	172.6, 172.0, 172.0
2	178.4, 178.4, 180.0	174.1, 174.1, 175.6
3	166.3, 166.6, 72.8	169.8, 171.7, 71.5
4	180.0, 175.7, 175.7	168.1, 171.3, 171.3
5	176.6, 175.6, 154.7	170.8, 172.0, 150.5
6	172.7, 149.0, 178.6	177.0, 145.2, 174.8
7	167.2, 169.6, 170.9	160.2, 169.9, 171.8
8	174.9, 165.5, 166.0	171.1, 168.3, 169.5
9	166.3, 163.4, 158.5	160.4, 165.7, 159.4

Structures of 1−9 in Solution. The steric effects of the bridgehead alkyl groups are found not only in the solid state but also in solution. For Cu(I) complexes **1**−**3**, the structures in solution are investigated by the electronic absorption spectra and ^{1}H NMR spectra, both of which are consistently explained on the basis of the structures in the solid state. For the Cu(II) complexes **4**−**9**, the electronic absorption and reflectance spectra and the ESR spectra revealed that the Cu(II) sulfate complexes **5** and **6** undergo structural changes in solution, while the structures of the Cu(II) sulfate complex **4** and the Cu(II) nitrate complexes **7**−**9** in solution are almost the same as those in the solid state.

The UV−vis absorption spectra of the Cu(I) complexes **1**−**3** show two distinct bands, which can be assigned to a ligand π−π* transition and a Cu(I) to ligand charge transfer (MLCT).[19,51,67] The π−π* bands of **1**−**3** appear in the range of 269−277 nm, unaffected by the bridgehead alkyl groups. On the other hand, the MLCT bands of **1** and **2** appear at 332 and 342 nm, respectively, indicating that the ligand field strength increases with increasing size of the bridgehead groups. The slight red shifts of MLCT bands in **2** as compared with **1** may be due to the shortening of the Cu−N_{py} bond distances shown in the crystal structures.

The ^{1}H NMR spectra of free ligands HL, MeL, and EtL and Cu(I) complexes **1**−**3** are measured to investigate the

(66) Addison, A. W.; Rao, T. N.; Reedijk, J.; van Rijn, J.; Verschoor, G. C. *J. Chem. Soc., Dalton Trans.* **1984**, 1349.

(67) Shimazaki, Y.; Yokoyama, H.; Yamauchi, O. *Angew. Chem., Int. Ed.* **1999**, *38*, 2401.

Table 8. Reflectance and Absorption Spectral Data for the d−d Transition Bands of **4**−**9** in CH_2Cl_2, MeOH−CH_2Cl_2 (1:10, v/v), and MeCN−CH_2Cl_2 (2:8, v/v)

cmpd	reflectance/ nm	λ_{max}/nm (ϵ/M^{-1} cm^{-1}) in CH_2Cl_2	in MeOH−CH_2Cl_2	in MeCN−CH_2Cl_2
4	710	710 (110)	698 (110)	697 (97)
5	750	614 (80)	616 (100)	616 (85)
6	720	580 (110)	663 (110)	599 (100)
7	710	720 (110)	698 (100)	704 (95)
8	680	690 (110)	696 (110)	700 (95)
9	710	753 (97)	697 (90)	701 (100)

steric effects of the bridgehead groups in solution. The 3- and 5-H_{py} are assigned on the basis of the cross-peaks between the 3-H_{py} and the bridgehead C*H*, C*H*$_3$, and C*H*$_2$-CH$_3$, and between the 5-H_{py} and the 6-C*H*$_3$ in the NOESY spectra (Supporting Information). All other H signals can be assigned without any additional technique. The chemical shifts of three signals due to the 3-, 4-, and 5-H_{py} atoms are almost constant in the free ligands, with slight shifts to the lower frequency region in MeL and EtL as compared to HL due to the electronic donation of the bridgehead alkyl groups. With complexation of the ligands, the H_{py} signals shift to the higher frequency region similarly to reported pyridine ligands.[68] The $\Delta\delta$ values [ppm] of the 3-, 4-, and 5-H_{py} with the complexation are 0.51, 0.21, and 0.22 for **1**, 0.90, 0.28, and 0.25 for **2**, and 0.33, 0.29, and 0.27 for **3**, respectively. The $\Delta\delta$ values 0.33−0.90 of the 3-H_{py} are larger than 0.21−0.29 of the 4- and 5-H_{py} and are largely different in **1**−**3**; 0.90 for **2** is the largest and 0.33 for **3** is the smallest. A similar tendency is found in the $\Delta\delta$ values of the bridgehead C*H*, C*H*$_3$, and C*H*$_2$CH$_3$ groups, which are 0.21, 0.36, and −0.02 for **1**, **2**, and **3**, respectively. These data suggest that the $\Delta\delta$ values reflect the contact between the bridgehead groups and the 3-H_{py} atoms. The large $\Delta\delta$ values of the 3-H_{py} and the C*H*$_3$ for **2** indicate the strong contact between the bridgehead methyl group and the 3-H_{py} atoms as shown in the crystal structure.[69] In contrast, the small $\Delta\delta$ values of the 3-H_{py} and the C*H*$_2$CH$_3$ for **3** may be due to the weak contact between the bridgehead ethyl group and the 3-H_{py} atoms. The structure of **3** in solution may be distorted to reduce the steric repulsion as in the solid state where two pyridine rings of EtL chelate in a bidentate mode and the other one is free from coordination though the pyridine rings are equivalent on the ^{1}H NMR time scale because of the rapid coordination exchange of the pyridine rings in solution due to labile character of the Cu(I) ion. From these results, it is concluded that the structures of **1**−**3** in the solid state may be kept in solution with the rapid coordination exchange of the pyridine rings.

The reflectance and the absorption spectral data for the d−d transition bands of the Cu(II) complexes **4**−**9** in CH_2Cl_2 are shown in Table 8. For the Cu(II) sulfate complexes of MeL and EtL, **5** and **6**, the absorption data, 614 and 580 nm, are largely different from the reflectance data, 750 and 720 nm, respectively, while for the Cu(II) sulfate complexes of HL, **4**, and the Cu(II) nitrate complexes **7**−**9**, the absorption data are close to the reflectance data. When MeOH or MeCN is added to the solutions, the d−d bands of **6** shift to the lower energy region, while those of other complexes are not so affected. The spectral change of **6** suggests the structural change in solution.

Table 9. Isotropic ESR Parameters of **4**−**9** in CH_2Cl_2−MeOH (10/1, v/v) in the Range 193−298 K and the Anisotropic ESR Parameters in Frozen Solutions at 77 K

cmpd	A_{iso} [G] 298 K	273 K	243 K	223 K	193 K	$A_{\|}$ [G] 77 K
4	54.0	52.3	55.2	53.9	54.8	163
5	72.4	71.1	70.3	69.9	62.1	154
6	80.1	78.9	79.3	79.7	71.1	182
7	45.8	47.8	47.4	48.6	47.8	160
8	45.4	45.8	45.8	49.1	45.4	154
9	67.4	74.0	69.9	72.8	68.7	149
			g_{iso}			$g_{//}$, $g_{\perp}$
4	2.15	2.15	2.16	2.15	2.15	2.29, 2.07
5	2.13	2.13	2.13	2.13	2.14	2.29, 2.06
6	2.13	2.12	2.12	2.15	2.11	2.25, 2.04
7	2.15	2.15	2.15	2.15	2.16	2.29, 2.07
8	2.17	2.14	2.15	2.15	2.14	2.29, 2.07
9	2.13	2.14	2.14	2.14	2.13	2.28, 2.07

Furthermore, we found unique temperature dependence of the isotropic hyperfine splitting (A_{iso}) values in the ESR spectra of **5** and **6**. The isotropic ESR parameters of **4**−**9** in CH_2Cl_2/MeOH in the range 193−298 K are shown in Table 9 along with the anisotropic ESR parameters in the frozen solutions at 77 K. The A_{iso} values of **5** and **6** are larger than those of **4** and **7**−**9** at 25 °C and are decreased with decreasing temperature. The relatively large A_{iso} values of **5** and **6** suggest that the coordination geometry might be distorted to square planar in solution.[70,71] This is consistent with the high-energy d−d bands in the absorption spectra of **5** and **6**. As shown already for **3** in the solid state and in solution, the bridgehead ethyl group induces the large distortion in the coordination structure to enforce one pyridine ring free from coordination. Thus, it is reasonable that the Cu(II) ion of **6** in solution assumes the square planar geometry with two pyridyl nitrogen atoms and two oxygen atoms of the sulfate ligand, and the other pyridine ring is free from coordination. The temperature-dependent A_{iso} values suggest that the coordination structures of **5** and **6** change with decreasing temperature. The $A_{||}$ value 154 G for the 77 K ESR spectrum of **5** is close to those of **4** and **7**−**9**, but that of 182 G for **6** is still larger than those of the other complexes, suggesting that in a frozen solution at 77 K, the Cu(II) ion of **5** assumes the trigonal bipyramidal geometry, but that of **6** still adopts a square planar geometry.

Electrochemical Properties of 1−9. The redox data of **1**−**9** are obtained from the cyclic voltammograms (CVs) and are shown in Table 10. The redox processes of **4** and **7**−**9** in CH_2Cl_2 are quasireversible, but those of **5** and **6** in CH_2Cl_2 are irreversible in which the cathodic peaks are very small. The sulfate chelates and the square planar geometries

(68) Gelalcha, F. G.; Schulz, M.; Kluge, R.; Sieler, J. *J. Chem. Soc., Dalton Trans.* **2002**, 2517.
(69) Dias, H. V. R.; Lu, H.-L.; Kim, H.-J.; Polach, S. A.; Goh, T. K. H. H.; Broening, R. G.; Lovely, C. J. *Organometallics* **2002**, *21*, 1466.
(70) Buchanan, R. M.; Wilson-Blumenberg, C.; Trapp, C.; Larsen, S. K.; Greene, D. L.; Pierpont, C. G. *Inorg. Chem.* **1986**, *25*, 3070.
(71) Hasty, E. F.; Colburn, T. J.; Hendrickson, D. N. *Inorg. Chem.* **1973**, *12*, 2414.

Table 10. Results from Cyclic Voltammetry Experiments[a]

cmpd	solvent	E_{pa} (mV)	E_{pc} (mV)
1	CH_2Cl_2	643	508
2	CH_2Cl_2	606	446
3	CH_2Cl_2	607	448
4	CH_2Cl_2	624	494
	20% MeCN/CH_2Cl_2	611	494
5	CH_2Cl_2	628	483
	20% MeCN/CH_2Cl_2	600	491
6	CH_2Cl_2	651	521
	20% MeCN/CH_2Cl_2	609	486
7	CH_2Cl_2	615	467
8	CH_2Cl_2	593	430
9	CH_2Cl_2	604	467

[a] All potentials are reported vs SCE at room temperature. Concentration of the supporting electrolyte TBAH is 0.1 M. Concentration of complex is 0.2 mM. Scan rate $\upsilon = 30$ mV s^{-1}.

in **5** and **6** in solution favor the Cu(II) states and may inhibit the reduction to the Cu(I) state. Upon addition of MeCN, the CVs of Cu(I) complexes **1**−**3** become extremely irreversible. The irreversible redox process may be caused by coordination of MeCN as a fifth ligand in the Cu(II) state.[26] In contrast, it was reported that the reversibility of CVs in a series of Cu(I) complexes of 6-MeO-substituted tripyridine ligands is improved upon addition of MeCN.[51] The opposite effect of MeCN may be explained by accessibility of MeCN. The 6-Me groups might inhibit the coordination of MeCN as a fifth ligand because the 6-Me groups provide greater steric hindrance than the 6-MeO groups as already shown. The incomplete binding of MeCN as a fifth ligand in the oxidation states of **1**−**3** may lead to irreversible CVs. The CVs of **7**−**9** become irreversible upon addition of MeCN, similar to those of **1**−**3**, while the reversibility in the CV of **6** is slightly improved. The irreversible CVs in **7**−**9** may be due to the ligand exchange of the nitrate with the MeCN. In **6**, the coordination of MeCN to the square planar Cu(II) ion is favorable for formation of the Cu(I) state, leading to improvement of reversibility of the CV. Differences of the redox potentials in **1**−**9** are small. The $E_{1/2}$ value of **1** is higher by ca. 50 mV than those of **2** and **3**, indicating that the bridgehead alkyl group may destabilize the Cu(I) state. This is consistent with the shortening of the Cu−N_{py} bond distances and the red shifts of the MLCT bands in **1**−**3**.

Conclusion

The structural modulation of copper complexes with subtle perturbation of the ligands is an essentially important approach for studying the Cu/O_2 chemistry. Many bidentate, tridentate, and tetradenate ligands have been used to investigate the Cu/O_2 chemistry, and modifications of the ligands, which lead to the structural modulation and functional control of the copper complexes, have been reported.[1−7] We have studied the Cu/O_2 chemistry by using the sterically hindered tripyridine ligand, HL. In this study, the sterically hindered tripyridine ligands having bridgehead methyl and ethyl groups, MeL and EtL, have been newly synthesized, and the structures of the Cu(I) and Cu(II) complexes of HL, MeL, and EtL in the solid state and in solution have been investigated. The bridgehead alkyl groups exert a dramatic effect on the coordination structures through the steric repulsion between the bridgehead alkyl groups and the 3-H_{py} atoms, leading to the pyridine shift. The pyridine shift shortens the Cu−N_{py} bond distances to strengthen the ligand field and enhances the steric hindrance of the 6-Me groups at the pyridine rings to affect coordination of the external ligands, MeCN, sulfate ions, and nitrate ions, leading to the distortion of the coordination structures. The bridgehead methyl group has the strongest contact with the 3-H_{py} atoms to induce the largest pyridine shift. The bridgehead ethyl group not only induces the pyridine shift but also affects the orientation of the pyridine rings, where the dihedral angles between the pyridine rings depend on the positioning of the methyl group in the bridgehead ethyl group as found in **3**, **6**, and **9**. Especially large conformational distortion of the pyridine ring is observed in **3**, where one of three pyridine rings is free from coordination and EtL chelates in a bidentate mode. In **6**, similarly, one pyridine ring may be free from coordination in solution because the spectral data suggest the copper coordination geometry is square planar, although in the solid state, three pyridine rings coordinate to form the distorted five-coordinate geometry. The modulations of the copper coordination structures with the bridgehead alkyl groups may give useful information for improving reversible O_2-binding of the Cu(I) complex of a sterically hindered hexapyridine ligand.

Acknowledgment. This work was supported by a Grant-in-Aid for Scientific Research (A) (14340210) from JSPS and the Aid of Doshisha University's Research Promotion Fund.

Supporting Information Available: X-ray crystallographic files in CIF format for **1**−**9**; Tables S1−S36, crystallographic experimental details, final atomic coordinates, thermal parameters, full bond distances and angles, ORTEP drawings, stereoviews, and one full-cells for **1**−**9**; Table S37, the average nonbonding interatomic distances, H···H (the 3-H_{py} atoms), N···N (the N_{py} atoms), and C···C (the 6-Me carbon atoms) for **1**−**9**; Figures S1−S6, the NOESY spectra of HL, MeL, EtL and the Cu(I) complexes **1**−**3**. This material is available free of charge via the Internet at http://pubs.acs.org.

IC026008M